Moore's curve structuring of ferromagnetic composite PE-NiFe absorbers

N. Fernez, Younès Arbaoui, A. Maalouf, A. Chevalier, P. Agaciak, Ludovic Burgnies, Patrick Queffelec, Vincent Laur, Eric Lheurette

Moore's curve structuring of ferromagnetic composite PE-NiFe absorbers

Cite as: J. Appl. Phys. **123**, 084902 (2018); https://doi.org/10.1063/1.5020367
Submitted: 22 December 2017 • Accepted: 09 February 2018 • Published Online: 26 February 2018

N. Fernez, Y. Arbaoui, A. Maalouf, et al.

Moore's curve structuring of ferromagnetic composite PE-NiFe absorbers

N. Fernez,[1] Y. Arbaoui,[2] A. Maalouf,[2] A. Chevalier,[2] P. Agaciak,[3] L. Burgnies,[1,4] P. Queffelec,[2] V. Laur,[2] and É. Lheurette[1]

[1]*Univ. Lille, CNRS, Centrale Lille, ISEN, Univ. Valenciennes, UMR 8520 - IEMN, F-59000 Lille, France*
[2]*Lab-STICC-UMR CNRS 6285, Université de Bretagne Occidentale, 6 Avenue Victor Le Gorgeu, CS 93837, 29238 Brest Cedex 3, France*
[3]*IRDL-FRE CNRS 3744, Université de Bretagne Occidentale, 6 Avenue Victor Le Gorgeu, CS 93837, 29238 Brest Cedex 3, France*
[4]*Université du Littoral Côte d'Opale, Rue Ferdinand Buisson, CS 80699, 62228 Calais Cedex, France*

(Received 22 December 2017; accepted 9 February 2018; published online 26 February 2018)

A ferromagnetic material involving nickel-iron particles embedded in a polyethylene matrix is synthesized and electrically characterized between 1 and 12 GHz. These measurements show the combination of electric and magnetic activity along with significant loss terms. We take benefit of these properties for the design of broadband electromagnetic absorbers. To this aim, we use a fractal structuring based on Moore curves. The advantage of etching patterns over metallic ones is clearly evidenced, and several pattern absorbers identified by their Moore's order iteration are designed and analyzed under oblique incidence. *Published by AIP Publishing.*
https://doi.org/10.1063/1.5020367

I. INTRODUCTION

Absorption of electromagnetic (EM) power remains a very interesting topic in wave science as well as a real challenge in wave engineering. Indeed, regarding the scientific side, an ideal absorbing layer should be able to stop the transmission and prevent the reflection of an EM wave whatever its frequency and incident angle. Regarding the engineering side, several solutions can be proposed in terms of materials and geometrical designs as a function of the targeted application, but it is obvious that an ideal absorber does not exist, as follows from the causality principle,[1] and each design results from a trade-off involving the absorption level, the bandwidth, the incident angle range and also the volume of the absorbing material. The latter first relies on the thickness of the absorbing layer and therefore on the added weight, which directly affects the performances of mobile systems, for example. Moreover, the cost of an absorbing device strongly depends on the required volume of the absorbing material. If this requirement may appear to be of second order from a scientific point of view, it can be decisive at low frequency applications because the layer thickness is proportional to the working wavelength, and therefore the requirement of a large volume of absorbing material tends to limit the development of mainstream applications targeting the isolation from mobile telecommunication signals such as GSM (0.9 and 1.8 GHz) or WiFi (2.45 GHz and 5 GHz). In order to absorb an EM wave, different ways can be followed. The first solution is the Dallenbach screen, which is based on the use of a composite lossy material.[2] Under the conditions of a destructive phase front occurring for an absorbing layer thickness around $\lambda_G/4$, where λ_G is the wavelength within the absorbing material, quasi-unit absorption can be achieved as a consequence of the dissipation of the EM power inside the lossy absorbing material.[3] The possibility to combine both dielectric and magnetic losses adds one degree of freedom in case of magneto-dielectric composite materials.[4] The limitation of Dallenbach screen relies on a resonance condition, which only guarantees significant absorption around the frequency

$$f_A = \frac{c}{4.T.\sqrt{real(\varepsilon_R.\mu_R)}}, \tag{1}$$

with c being the light velocity; ε_R and μ_R the complex relative permittivity and the permeability of the absorbing layer, respectively; and T its thickness. Please note that Eq. (1) is valid only in case of weak dispersions of the constitutive parameters. Absorption bandwidth is therefore inversely proportional to the resonance quality factor. An alternate design of the Dallenbach absorber, also termed Salisbury screen,[5] uses a resistive film on top of a low-loss dielectric layer instead of a bulk lossy one. Starting from the Dallenbach idea, several solutions may be introduced in order to broaden the absorption bandwidth. In its principle, the only tuning parameters of the Dallenbach screen are the complex permittivity and permeability values which can be either constant or frequency dependent over the absorption bandwidth. In order to broaden the absorption bandwidth, efforts can be focused on the material dispersion by taking benefit of permeability relaxation occurring in high susceptibility spinel ferrites. Technically, this approach requires a challenging process based on the stacking of thin films.[6] Assuming weak dispersions of the constitutive parameters, the goal of any improvement of the Dallenbach concept is the introduction of additional materials or geometrical parameters which means that new degrees of freedom aimed at engineering the absorption spectrum. The first idea consists of stacking several layers, each characterized by its own complex constitutive parameters. This design, inspired from a Jaumann absorber,[7] is valid when the potential thickness increase is not a critical issue. Another possibility is to use a filtering surface, also termed FSS for Frequency Selective Surface, on top of the absorbing layer.[8] Along with the emergence of

metamaterials in various fields of wave science, this concept has also been applied to the design of EM absorbers from microwaves to optics. The basic idea has been to take benefit of short scale localization by means of high quality electric or magnetic field resonances to extend the properties of geometrically structured absorbers. For optics, the possibility to introduce artificial magnetism brought new degrees of freedom.[9–11] For microwaves, localizing fields over a sub-wavelength thickness paves the way for the design of low-profile light-weight absorbing layers, thus satisfying a requirement common to many application fields such as embedded electronics, or indoor shielding from EM pollution. Nevertheless, resonance mechanisms implying narrow-band responses remain one of the major drawbacks of the metamaterial approach. This can be alleviated by introducing multi-scale resonant patterns, either in the plane of the structure (parallel structuring)[12,13] or in the propagation plane (perpendicular structuring).[10] Physically, the perpendicular structuring is often preferred to the parallel one since it does not introduce super-cell effects at the origin of parasitic diffraction under oblique incidence. However, introducing a multi-scale structuration along the propagation direction means increasing the thickness of the absorbing layer, thus leading to a trade-off between bandwidth enlargement and thickness. From these few considerations related to the resonance quality factor, the absorbing bandwidth and the thickness of the absorbing layer, we propose to study the behavior of a ferromagnetic composite material (ferrocomposite) structured by means of Moore's curve patterns. Prior to this, synthesis and EM characterization of the ferrocomposite material is detailed in Sec. II.

II. SYNTHESIS AND ELECTRICAL CHARACTERIZATION OF PE-NiFe MATERIAL

Various volume fractions of nickel-iron ferromagnetic particles are diluted in a polymeric polyethylene (PE) matrix according to the following process.[14] Composites were prepared from a linear polyethylene matrix supplied by Enichem (Flexirene® FG 20F). The filler used in this study was nickel-iron powder supplied by Goodfellow ($Ni_{81}Fe_{19}$® NJ016020). The first PE matrix and NiFe powders were simultaneously mixed using a DSM Xplore lab twin screw extruder at 200 °C and a screw rotational speed of 50 rpm. Then, the resulting material has been cryogrinded and molded at the temperature of 200 °C under a pressure force of 25 MPa. This process insures a uniform dispersion of micrometric ferromagnetic charges with an average diameter D_{moy} equal to 5 μm (Ref. 14), as illustrated by the SEM picture of Fig. 1. In this example, the volume concentration of $Ni_{81}Fe_{19}$ particles is 40%.

The use of ferrocomposites for the design of broadband absorbers requires an accurate awareness of its complex constitutive parameters over the whole frequency band of interest. To this aim, the synthesized composites have been inserted into a coaxial cell and characterized by means of a Vector Network Analyzer (VNA). At first, the coaxial airline (APC7 standard) was measured in order to evaluate insertion losses in the empty cell. Then, a toroidal sample of

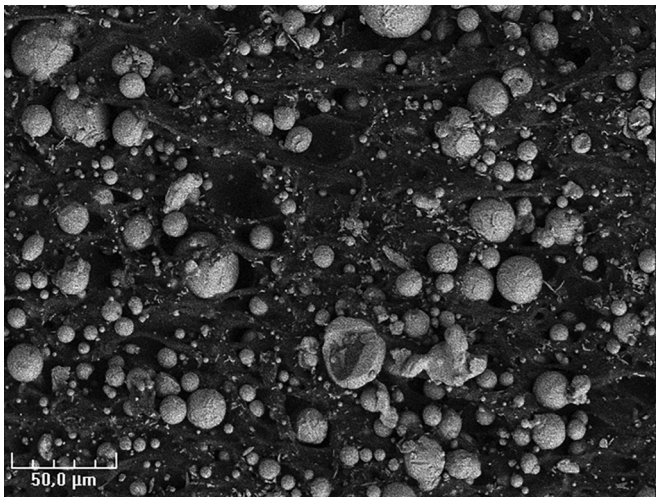

FIG. 1. SEM picture of the PE-NiFe composite including 40% of NiFe particles in a PE matrix.

the material under test, with an inner diameter of 3.04 mm and an outer diameter of 7 mm, was inserted into the coaxial line. S-parameters of the coaxial line filled with the sample were computed, thanks to the Nicolson-Ross Weir (NRW) procedure[15] to extract electromagnetic properties of the composite. The concentration of $Ni_{81}Fe_{19}$ needs to satisfy a trade-off between the targeted EM properties, structural characteristics such as the homogeneity of the composites, and mechanical properties. Taking these requirements into account, we focused on PE(60%)-NIFe(40%), whose experimental complex effective permittivity and permeability are plotted in Fig. 2 in the 1–12 GHz frequency band. The real part of permittivity is larger than 9, all over the frequency band of interest. Since the thickness of the absorbing layer strongly depends on the wavelength inside the absorbing material as previously mentioned, high values of permittivity are welcome. In addition, the imaginary part of permeability starting from 1.5 at 1 GHz and decreasing down to 0.5 at 12 GHz remains high all over the frequency band of interest. The dispersion of this loss term appears favorable when targeting a broadband absorption behaviour.

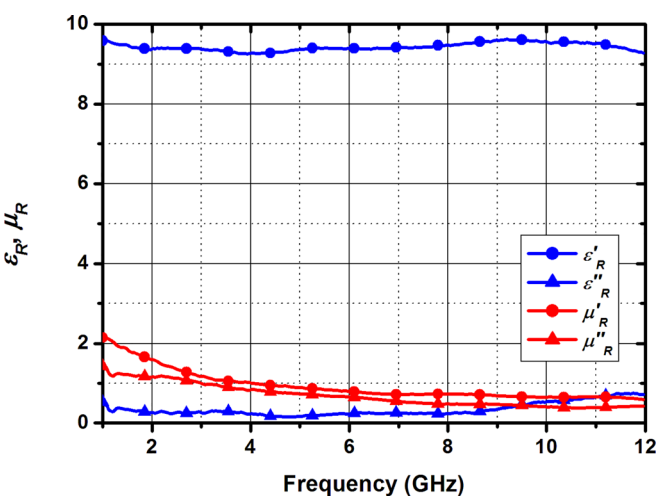

FIG. 2. Measured real and imaginary parts of the permittivity and permeability spectra of PE(60%)-NiFe(40%).

Considering the values of permittivity and permeability of the PE(60%)-NiFe(40%) ferrocomposite, Eq. (1) points out a trade-off between the low absorption frequency (f_A) and the reasonable absorbing layer thickness (T). All the numerical simulations discussed in Secs. II, IV and V of this article have been performed by means of the frequency solver of *CST Microwave Studio*, and the PE(60%)-NiFe(40%) ferrocomposite material has been modeled using the measured dispersion curves given in Fig. 2. The absorption behavior of a 10 mm thick PE(60%)-NiFe(40%) plain layer back-grounded with a perfect conductor is reported in Fig. 3. Assuming that transmission is forbidden due to the presence of the ground-plane, power absorbance can be easily determined from Eq. (2), where R stands for the magnitude of the reflection coefficient.

$$A = 1 - R^2. \tag{2}$$

Under normal incidence ($\theta = 0°$) and at a slight oblique incidence ($\theta < 10°$), a unit peak absorption at typically 1.6 GHz can be clearly evidenced. This peak relies on the $\lambda_G/4$ resonance phenomenon previously described. When frequency increases, absorbance decreases, but remains greater than 0.6 up to 12 GHz. In order to analyze the absorption behavior under oblique incidence, we considered separately the TE (electric field vector remains parallel to the layer plane) and the TM (magnetic field vector remains parallel to the layer plane) polarization cases (see Fig. 3).

Under TE polarization, the absorption gradually decreases as a function of the incidence angle down to an extra resonance plateau of 0.2 at $\theta = 80°$. Under TM polarization, the extra resonance absorption level tends to increase and reaches a maximum value slightly lower than 1 for an incident angle of 70°. This is the consequence of the well-known Brewster angle (θ_B) phenomenon which predicts a zero reflection condition around 7 GHz for an incident angle of 75° according to Eq. (3), where n_2 and n_1 stand for the refractive index of the absorbing layer and air ($n_1 = 1$), respectively,

$$\tan(\theta_B) = \frac{n_2}{n_1}. \tag{3}$$

In the following, we introduce the Moore pattern as a way to overcome the resonance behavior of the plain layer by keeping the absorbance level as high as possible over the whole frequency band of interest.

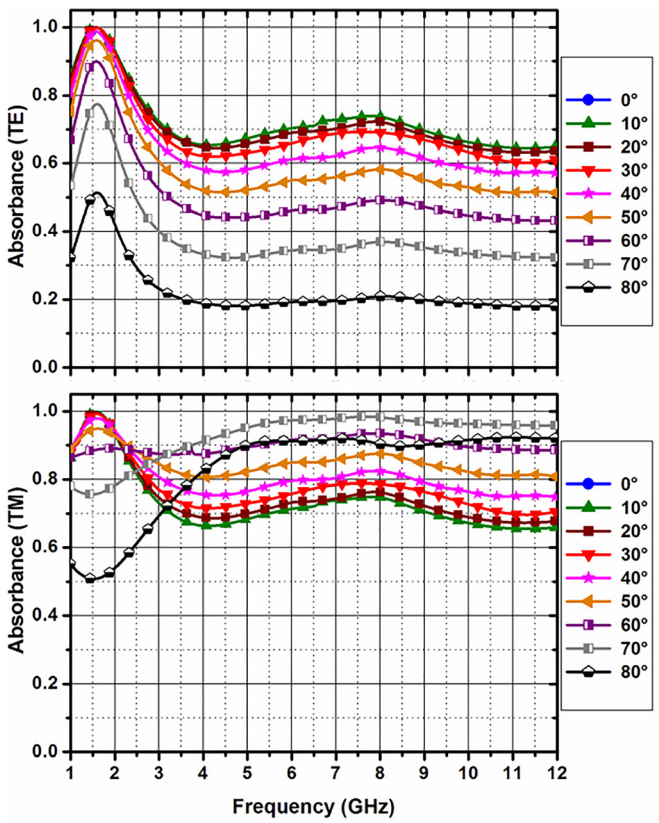

FIG. 3. Absorbance spectra of a plain 10 mm thick ferrocomposite layer for various incidence angles in TE (top) and TM (bottom) polarizations.

III. MOORE'S CURVE STRUCTURATION APPROACH

Moores's curve pattern is a continuous fractal space filling curve.[16] It can be understood as a loop version of the Hilbert curve, and can be expressed by the following rewrite system, the so-called L-system, introduced back in 1968 by the theoretical biologist A. Lindenmayer in order to model the grow process of plants. Moore's rewrite system can be described by the following axiom:

$$\mathrm{LFL} + \mathrm{F} + \mathrm{LFL}, \tag{4}$$

and production rules (5) and (6)

$$\mathrm{L} \rightarrow -\mathrm{RF} + \mathrm{LFL} + \mathrm{FR}-, \tag{5}$$

$$\mathrm{R} \rightarrow +\mathrm{LF} - \mathrm{RFR} - \mathrm{FL}+, \tag{6}$$

where L and R are two variables, and F, +, − three constant meaning "draw forward," "turn left 90°" and "turn right 90°," respectively. A more complete description of the L-system can be found in Ref. 17.

Following this rewrite process, an algorithm was implemented in order to generate Moore's pattern without any fundamental order limit. As an example, the resulting Moore patterns from order one to four are depicted in Fig. 4. The areas surrounded by the Moore curves are depicted in blue color. For the first order, this area is equal to

$$A_1 = \frac{p^2}{4}, \tag{7}$$

where p is the period of the unit-cell.

The Moore area determination can be generalized to the nth order using the formula

$$A_n = p^2\left[\frac{1}{4} + 3\sum_{i=2}^{n}\frac{1}{4^i}\right], \tag{8}$$

in which a geometric series of common ratio equal to $\frac{1}{4}$ can be identified, thus leading to the final expression

$$A_n = p^2\left[\frac{1}{2} - \frac{1}{4^n}\right]. \tag{9}$$

Let us introduce a quantity termed as the Moore filling fraction

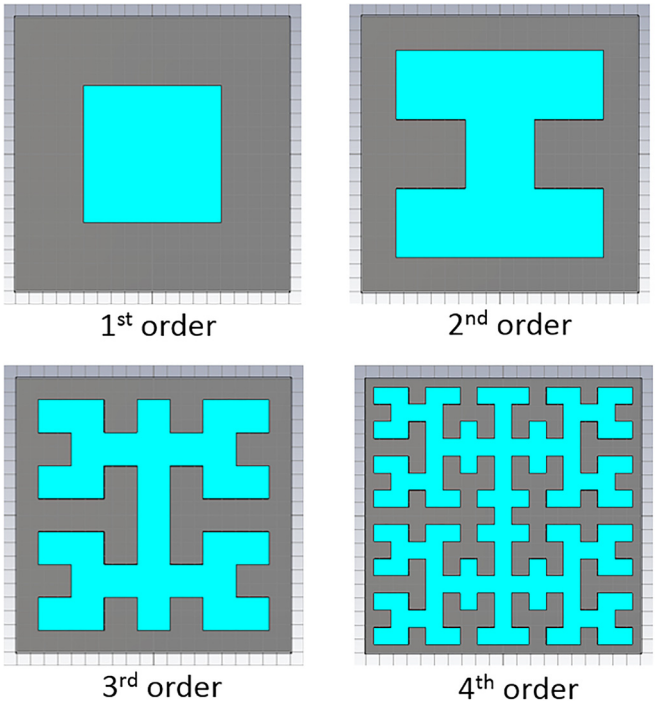

FIG. 4. Elementary cell Moore curve patterns from the first to the fourth order. In every case, the unit cell is a 20 cm edge square.

$$ff_n = \frac{A_n}{p^2} \times 100\%, \tag{10}$$

which will be considered for the analysis of Moore structured absorbing layers. From Eqs. (9) and (10), it is obvious that starting from 25% for the first order, the nth order ff_n rapidly converges on 50% when increasing Moore's iteration.

These patterns have been reproduced on PE-NiFe absorbers with the following characteristics: A layer of PE-NiFe is back-grounded with a perfect electric mirror. The thickness of this plain layer is equal to 10 mm in order to get an intrinsic resonance at the beginning of the frequency band according to Eq. (1). The idea is to broaden this intrinsic response by the introduction of additional modes whose number increases as a function of Moore's pattern order. The elementary cell is a 20 cm edge square shape. According to Moore's process, this elementary cell is divided into 4^n square sub-domains and Moore's curve joins the centers of this sub-domains according to the rewrite process described above. Consequently, the first order pattern consists of a $10 \times 10\,cm^2$ square shape centered in the $20 \times 20\,cm^2$ elementary cell, whereas the width of the fourth order pattern strips is 12.5 mm.

From an EM perspective, structuring a plain layer of material means locally modifying its EM boundaries following a specific pattern. This can be done by using either a metallic pattern on top of the plain PE-NiFe layer or by cutting the PE-NiFe out following the same pattern. For the sake of comparison, these two approaches, namely metallic and etched structuration, have been initially considered in the following numerical analysis. It is important to note that our main goal is to broaden the absorption bandwidth by introducing additional features in the frequency spectrum. This differs from other works, where the use of cutting out structures is proposed in order to improve impedance matching with air around a single resonance frequency.[18]

IV. MOORE'S CURVE PATTERNING: METAL VERSUS ETCHING STRUCTURATION

As referred to the patterns plotted in Fig. 4, in the case of metal structuration, the metallic patch in blue color is deposited on top of a back-grounded plain PE-NiFe layer in grey color, whereas in the case of etching structuration, the PE-NiFe patch in blue color is deposited onto a ground plane in grey color. The metallic patch is 35 μm thick, and considering the frequencies of interest in the domain of microwaves, both metallic patch and ground planes have been modeled as perfect conductors. The response of an infinite periodic structure is analyzed under normal incidence using a Floquet injection port and an elementary cell bounded by periodic conditions. The absorbance spectra of the metal and etched Moore patterns are reported in Fig. 5. For the sake of comparison, we also inserted the response of the plain PE(60%)-NiFe(40%) layer in a solid black curve. The metal structuring does not improve the absorption of the PE-NiFe plain layer since one does not take benefit of the so-called magnetic resonance at

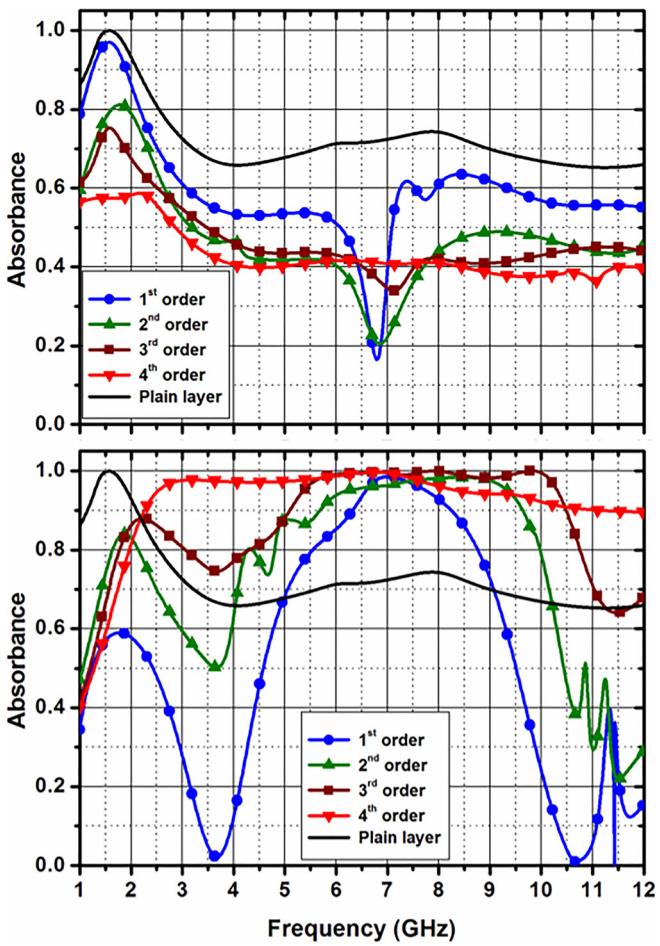

FIG. 5. Compared absorption spectra for a 10 mm PE(60%)-NiFe(40%) layer structured by metal-covered (top) and etched (bottom) Moore's pattern. The response of a plain bare 10 mm layer is also plotted in a solid black line.

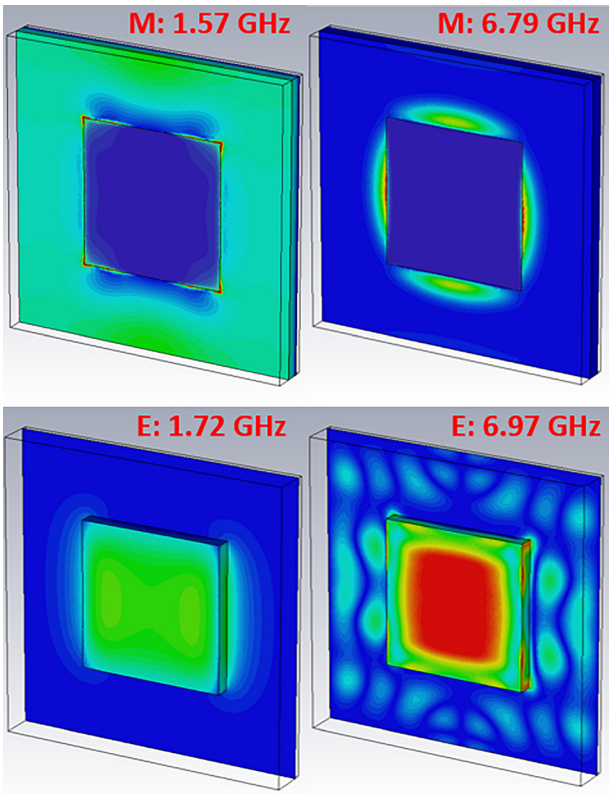

FIG. 6. Poynting vector magnitude filed maps for the 1st order Moore pattern defined by metallization [top: linear scale between 0 (blue color) and 100 W/m^2 (red color)] and etching [bottom: linear scale between 0 (blue color) and 126 W/m^2 (red color)].

the origin of unit absorbance level in Metal Insulator Metal (MIM) structures.[19] Such an absorption mechanism is mainly based on the quality factor of the open resonator defined by the metallic patch facing the ground plane through an insulating layer.[13] Yet, it should be noted that the quality factor would be weak consecutively to the high values of permittivity and permeability imaginary parts. Without this magnetic resonance mode, the metallic patterns behave as an electric mirror preventing the penetration of the electromagnetic wave into the ferromagnetic layer thus leading to an increase of the reflectivity. This mechanism is pointed out in Fig. 6, which reports the Poynting vector magnitude field maps in the case of metallic (M) and etched (E) 1st order Moore structures. Indeed, the electric mirror behavior of the metallic patch induces a shadowing effect corresponding to a near-zero power flow area at the absorbance peak frequency ($f = 1.57$ GHz). For the lowest Moore orders, typically from 1 to 3, a dip in the absorbance spectrum occurs around 7 GHz due to the resonant nature of the finite size pattern (see Fig. 6, M: 6.79 GHz). This dip is the consequence of a resonance in the reflectivity which also occurs when the PE-NiFe layer is not back grounded, thus accrediting the assertion of a FSS resonance preventing the EM wave from coupling with the ferrocomposite layer. Out of this dip, the absorbance level tends to decrease with the Moore order as a consequence of an increase of the metallic surface. Actually, as previously mentioned, this surface increases rapidly at the lowest Moore's orders and tends to the limit of 50% for the highest orders. This explains why the absorbance plateau level tends to the same value (~0.4) both for orders 4 and 5. To summarize the metal Moore's structuring, increasing reflectivity degrades the absorption performance with respect to the plain 10 mm thick PE-NiFe layer.

On the contrary, as illustrated in the bottom graph of Fig. 5, a gradual increase of the absorption bandwidth is clearly evidenced in case of etched Moore structures. Let us recall that strictly, the same dimensional data have been used to define the metallized and etched patterns. Considering this, one can say that the open air boundary condition applied on top and on the edges of the etched ferrocomposite material helps in coupling and localizing the EM energy inside the PE-NiFe where it can be efficiently dissipated due to the high level of magnetic loss. This process is illustrated in the bottom part of Fig. 6. It should be noted that the same Poynting vector magnitude scale has been used for both frequencies. The resonance phenomenon is then pointed out at $f = 6.97$ GHz. In contrast, the map of the absorbance peak at $f = 1.72$ GHz mainly illustrates the plain layer response. This is why the peak value around 1.72 GHz decreases down to 0.6 due to the reduced volume of lossy PE-NiFe, as a consequence of the etching process.

When increasing Moore's pattern order, the peak absorbance located at 7 GHz gradually broadens towards high frequencies until the absorbance level reaches 0.9 at 12 GHz. Moreover, the weak absorbance observed around 3.5 GHz for the order 1 tends to increase when complicating the Moore pattern, thus contributing to the bandwidth enhancement at low frequencies. The low frequency absorbance improvement is directly related to an increase of the lossy ferrocomposite volume, since the PE-NiFe relative area tends to 50% from the 4th order Moore pattern. In order to better understand this absorbance progress from a distribution around the 7 GHz peak for the first order to a 90% plateau extending from 2.3 up to 12 GHz, a polar representation of the reflection coefficient can help to identify the resonance modes. Actually, due to the loss level of PE-NiFe, the quality factor of these resonances would be too small to clearly locate resonance peak frequencies in the absorbance spectrum of Fig. 5. To circumvent this difficulty, the reflected phase evolution brings additional information by relating phase jumps and resonance signatures. Therefore, we plotted a polar diagram of reflectivity in Fig. 7, where the radius represents the magnitude and the angle represents the phase of the reflection coefficient. Please note that this reflection coefficient is referenced in the top plane of the structured PE-NiFe. From this plot, we pointed out its characteristic features. Point 2 for a frequency $f_2 = 6.79$ GHz is the closest to the center of the polar plot, and is related to the maximum of absorbance. The three other marked points, namely $f_1 = 4.76$ GHz, $f_3 = 8.72$ GHz and $f_4 = 10.88$ GHz, by indicating the curve loop features, are clearly related to phase jumps and therefore to resonance mechanisms. As expected, the field maps plotted in Fig. 7 show a uniform repartition of the power flow at $f_2 = 6.79$ GHz since no resonance phenomenon can be evidenced in the polar plot. On the contrary, localizations of the power flow over specific branches of the 4th order Moore pattern can be evidenced at $f_1 = 4.76$ GHz, $f_3 = 8.72$ GHz and $f_4 = 10.88$ GHz due to the resonances identified by curve loops in the polar plot. These resonances although not very pronounced, as a

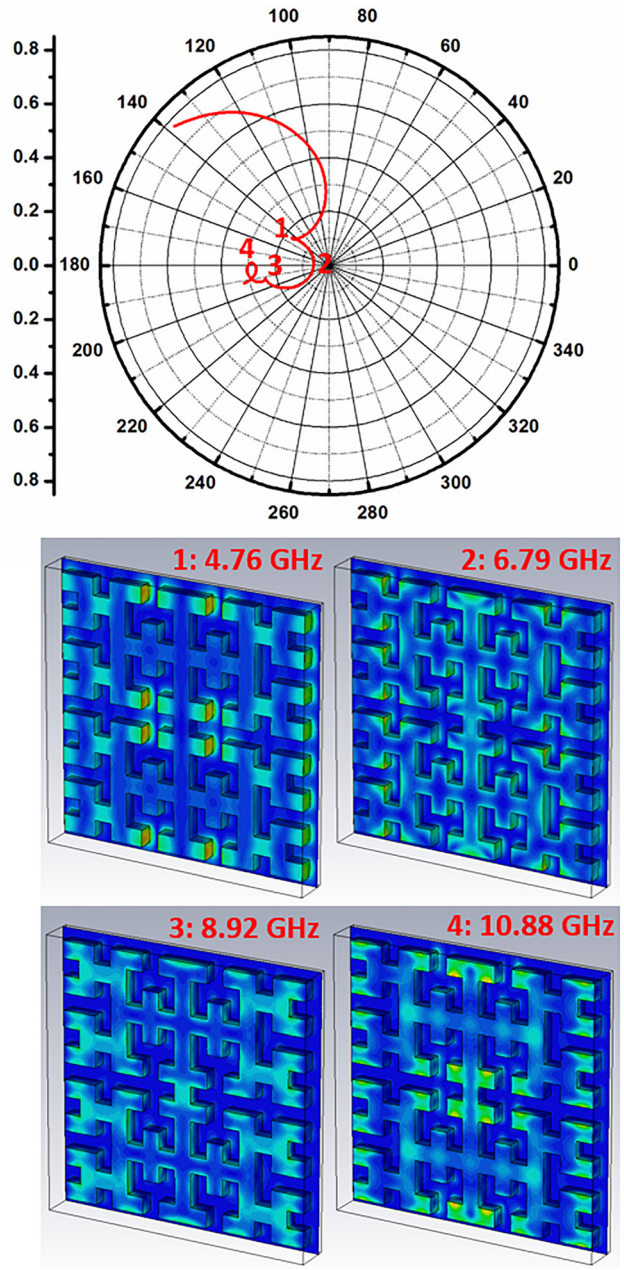

FIG. 7. Polar diagram of the reflection coefficient over the 1–12 GHz frequency band for the 4th order etched structure and Poynting vector magnitude field maps for the four frequencies indexed in the polar diagram, 1: 4.76 GHz, 2: 6.79 GHz, 3: 8.92 GHz and 4: 10.88 GHz. The linear scale ranges from 0 (blue color) up to 200 W/m^2 (red color).

consequence of the dielectric and especially magnetic loss terms, are at the origin of the relative absorbance band broadening of up to $\Delta f/f_0 = 130\%$ around the central frequency $f_0 = 7.15$ GHz for the 4th order Moore structure. These values are given for an absorption rate of 90%, often considered as an engineering reference.

In Sec. V, the absorbance of a high order Moore's pattern has been considered under oblique incidence, and the relevance of in-plane geometric parameters is discussed.

V. OBLIQUE INCIDENCE ANALYSIS AND DISCUSSION

Here, we analyze the response of the Moore structures under oblique incidence by focusing on the highest orders which are most promising in terms of absorption bandwidth. Absorbance spectra are plotted in Fig. 8 for the 4th and 5th orders Moore structures illuminated with a TE- or TM-polarized wave. Like previously observed on a plain ferro-composite layer (see Sec. II), the TM polarization is much more robust to oblique incidence than the TE one, due to the contribution of the Brewster angle estimated at around 75°.

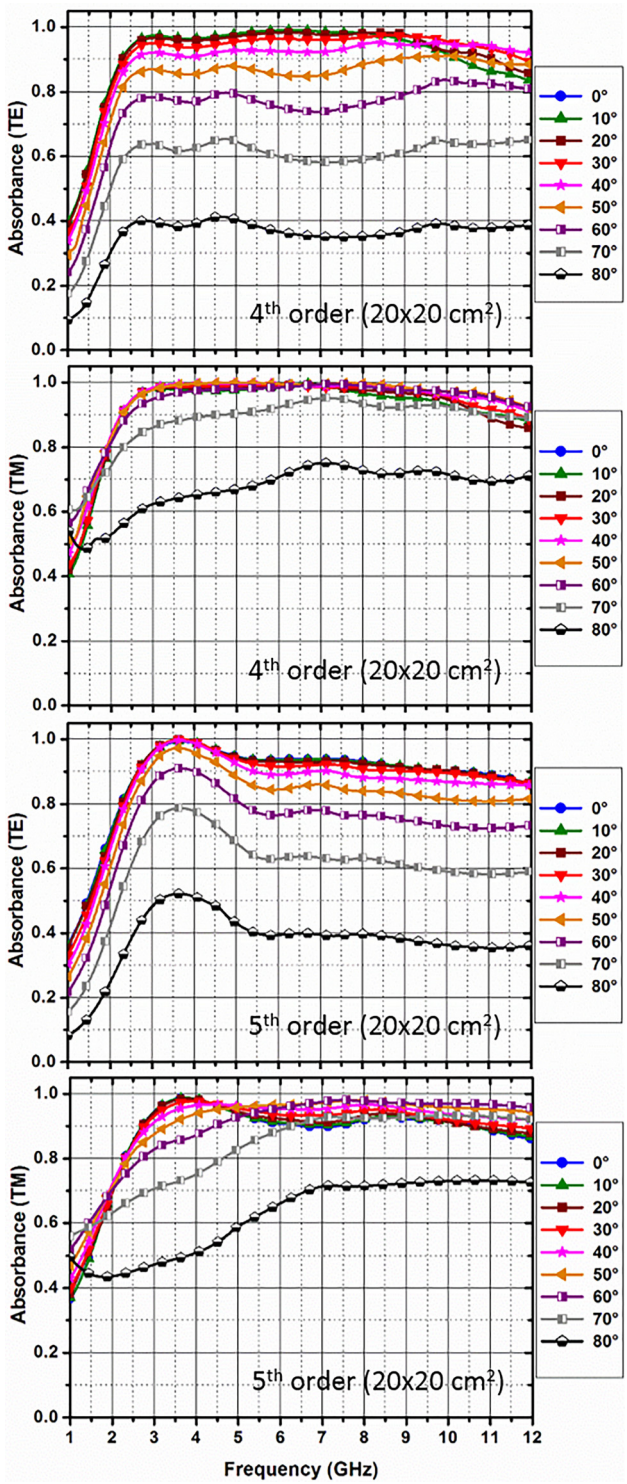

FIG. 8. Absorbance spectra under oblique incidence for the 4th and 5th order Moore patterns from top to bottom: 4th order TE mode, 4th order TM mode, 5th order TE mode, and 5th order TM mode. The unit-cell area is a 20 cm edge square.

Nevertheless, with a targeted absorbance level of 90%, even the TE polarization shows interesting performances until the limit angle of 40°. For the TM polarization, this limit angle can be as high as 70°. These values correspond to the 4th order Moore structures whose oblique incidence spectra are given on the top part of Fig. 8.

In comparison with the same unit-cell area, the absorption level of the 5th order Moore structure tends to decrease when frequency is higher than 3.5 GHz, again with a limited incident angle devaluation under TM polarization (see the bottom plots of Fig. 8). This behavior does not directly describe a weaker absorbance due to the 5th order pattern itself. Actually, when increasing the Moore order with a constant unit cell area, the width of the ferrocomposite strips tends to decrease along with the width of the grooves. More exactly, in accordance with the algorithm detailed in Sec. III, those widths are divided by a factor 2 at each Moore's curve iteration. As an example, for a $20 \times 20\,cm^2$ unit cell, both the strip and groove widths are equal to 12.5 mm for the 4th order and 6.25 mm for the 5th order patterns. As a consequence, the coupling efficiency of the impinging wave with the structured ferrocomposite layer is reduced.

This assertion is confirmed by the plots of Fig. 9, in which the unit cell area has been multiplied by 4 thus leading to an identical strip and groove width (12.5 mm) with respect to the value obtained for the 4th order $20 \times 20\,cm^2$ unit-cell previously commented. In this case, the curves obtained for the 5th order Moore pattern ($40 \times 40\,cm^2$ area unit cell) (top graphs of Fig. 9) are almost identical to the ones observed for the $20 \times 20\,cm^2$ area unit cell 4th order structure (top graphs of Fig. 8). Therefore, increasing Moore's curve order from 4th to 5th does not contribute to broaden the absorption band. This can be generalized to a higher order, as it has been checked on the 6th order which produces the same spectral response (not plotted here) provided that the unit cell area increased to $80 \times 80\,cm^2$ in order to keep the strip and groove widths equal to 12.5 mm. From this assessment, one can wonder if it is possible to achieve a similar absorption bandwidth by reducing the unit cell area of the 3rd order Moore pattern down to $10 \times 10\,cm^2$ in order to keep the strip and groove widths equal to 12.5 mm.

Such a structure has also been simulated, and the oblique incidence spectra are given in the bottom part of Fig. 9. Actually, the 90% absorption bandwidth significantly increased with respect to the graph plotted in Fig. 5, for which the strip and groove widths are equal to 25 mm. As a conclusion, this geometrical parameter is a key factor for optimizing the coupling of the impinging wave with the structured ferrocomposite layer. Nevertheless, the spectra obtained for the 3rd order $10 \times 10\,cm^2$ structure cannot be rigorously superimposed with the previous ones (4th order $20 \times 20\,cm^2$ and 5th order $40 \times 40\,cm^2$), and the absorption bandwidth is slightly reduced.

The reflectivity polar plots related to these three structures (3rd order $10 \times 10\,cm^2$, 4th order $20 \times 20\,cm^2$ and 5th order $40 \times 40\,cm^2$) are given in Fig. 10. First, it should be noted that the curves are practically superimposed from

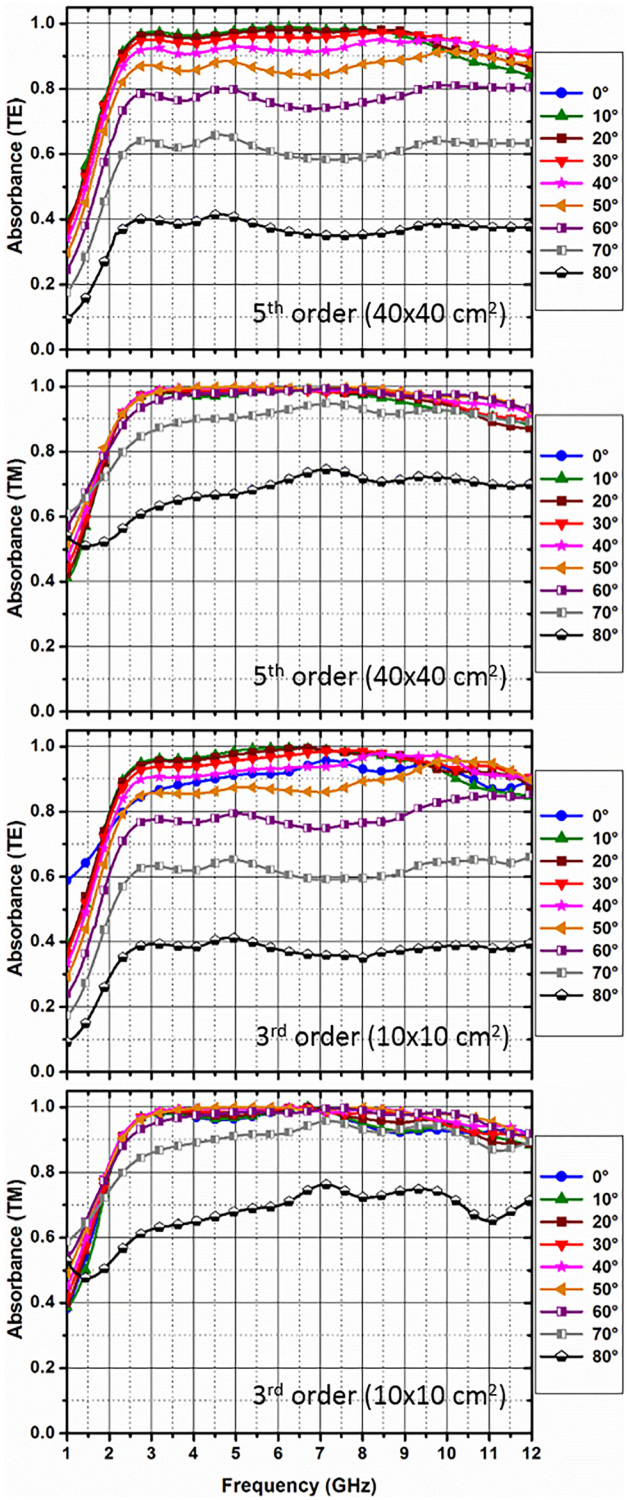

FIG. 9. Absorbance spectra under oblique incidence for the 5th ($40 \times 40\,cm^2$) and 3rd order ($10 \times 10\,cm^2$) Moore patterns from top to bottom: 5th order TE mode, 5th order TM mode, 3rd order TE mode, and 3rd order TM mode.

1 GHz up to the first resonance at f = 4.76 GHz (see Fig. 7). Then, the reflectivities slightly differ above this resonance frequency. In particular, the 3rd order one crosses the center of the plot revealing a zero reflectance situation. Nevertheless, the most important information is the fact that no additional resonance can be evidenced for the 5th order

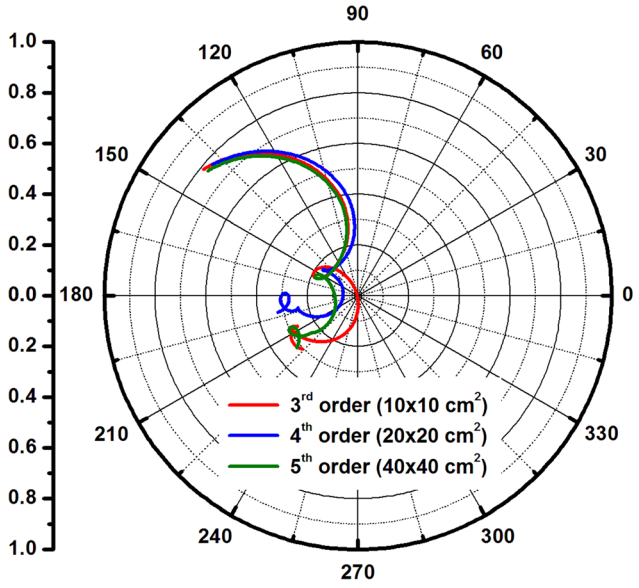

FIG. 10. Polar diagram of the reflection coefficient over the 1–12 GHz frequency band for the 3rd, 4th and 5th order Moore patterns.

structure. This explains why complicating the Moore pattern up to the 5th order does not contribute to further broaden the absorption band. In addition, it should be noted that for the last three structures, the Moore area filling fractions defined by Eq. (10) $ff_3 \sim 48.4\%$, $ff_4 \sim 49.6\%$ and $ff_5 \sim 49.9\%$ are quite similar, thus leading to an equivalent volume of the absorbing material. However, as previously mentioned, when targeting a constant strip width equal to 12.5 mm, the area of the unit-cell is multiplied by 4 at each Moore's curve iteration. For a given absorbance spectrum, the opportunity to choose the period of the structure array and to evolve towards an aperiodic design for the highest Moore's orders may be of great interest for practical implementation.

VI. SUMMARY AND CONCLUSIONS

A PE-NiFe ferromagnetic composite material has been successfully synthesized. For a NiFe concentration of 40%, experimental characterization demonstrated a real part of permittivity greater than 9 along with a real part of permeability averaging 1, and a magnetic loss tangent varying between 0.6 and 0.8 over the 1–12 GHz frequency band. A numerical analysis of this composite structuration by means of fractal Moore's curve etching showed the possibility to achieve a 90% absorption relative bandwidth as high as $\Delta f/f_0 = 130\%$ around the central frequency $f_0 = 7.15$ GHz. In addition, this broadband absorption has been found to handle a wide domain of incidence angle. The simulations conducted under oblique incidence showed a relative invariance of the absorption spectra with respect to Moore's iteration as long as Moore's order is at least equal to 4, and the Pe-NiFe strip width is kept constant (12.5 mm). This allows using the periodicity of the array as a degree of freedom in practical structures and paves the way for the design of aperiodic absorbers.

ACKNOWLEDGMENTS

N. Fernez would like to thank the Direction Générale de l'Armement (DGA) and Université de Lille for his Ph.D. co-funding. This research was financially supported by l'Agence Nationale de la Recherche (ANR) in the framework of ANR ASTRID 3DRAM (ANR-14-ASTR-0006-01) project.

[1]V. S. Asadchy, I. A. Fanaiayeu, Y. Ra'Di, S. A. Kharkhomov, I. V. Semchenko, and S. A. Tretyakov, Phys. Rev. X **5**, 031005 (2015).
[2]M. Oyharçabal, T. Olinga, M.-P. Foulc, S. Lacomme, E. Gontier, and V. Vigneras, Compos. Sci. Technol. **74**, 107 (2013).
[3]W. Dallenbach and W. Kleinsteuber, Hochfrequenztech. Elektroakust. **51**, 152 (1938).
[4]K. J. Vinoy and R. M. Jha, Sadhana **20**, 815 (1995).
[5]R. L. Fante and M. T. McCormack, IEEE Trans. Antennas Propag. **36**, 1443 (1988).
[6]P. Chen, R.-K. Li, Y. Gu, Y. Shi, and R. Wu, J. Magn. Magn. Mater. **349**, 259 (2014).
[7]B. Chambers and A. Tennant, Electron. Lett. **30**, 1530 (1994).
[8]S. N. Zabri, R. Cahill, and A. Schuchinsky, Electron. Lett. **51**, 162 (2015).
[9]P. Bouchon, C. Koechlin, F. Pardo, R. Haïdar, and J.-L. Pelouard, Opt. Lett. **37**, 1038 (2012).
[10]F. Ding, Y. Cui, X. Ge, Y. Jin, and S. He, Appl. Phys. Lett. **100**, 103506 (2012).
[11]M. Hedayati, F. Faupel, and M. Elbahri, Materials **7**, 1221 (2014).
[12]A. Sellier, T. V. Teperik, S. N. Burokur, G. Sabanowski, G.-P. Piau, and A. de Lustrac, Appl. Phys. A **117**, 739 (2014).
[13]N. Fernez, L. Burgnies, J. Hao, C. Mismer, G. Ducournau, D. Lippens, and E. Lheurette, "Radiative Quality Factor in Thin Resonant Metamaterial Absorbers," IEEE Trans. Microwave Theory Tech. (to be published).
[14]Y. Arbaoui, P. Agaciak, A. Chevalier, V. Laur, A. Maalouf, J. Ville, P. Roquefort, T. Aubry, and P. Queffelec, J. Mater. Sci. **52**, 4988 (2017).
[15]W. B. Weir, Proc. IEEE **62**, 33 (1974).
[16]H. Sagan, *Space-Fill. Curves* (Springer, New York, NY, 1994), pp. 9–30.
[17]P. Hazdra and M. Mazanek, Radioengineering **15**, 18 (2006).
[18]H.-S. Cho and S.-S. Kim, J. Appl. Phys. **117**, 17A311 (2015).
[19]J. Hao, R. Niemiec, L. Burgnies, E. Lheurette, and D. Lippens, J. Appl. Phys. **119**, 193104 (2016).